Nanotechnology

PAPER • OPEN ACCESS

Nanoheteroepitaxy of Ge and SiGe on Si: role of composition and capping on quantum dot photoluminescence

To cite this article: Diana Ryzhak *et al* 2024 *Nanotechnology* **35** 505001

OPEN ACCESS
IOP Publishing
Nanotechnology
Nanotechnology **35** (2024) 505001 (10pp)
https://doi.org/10.1088/1361-6528/ad7f5f

Nanoheteroepitaxy of Ge and SiGe on Si: role of composition and capping on quantum dot photoluminescence

Diana Ryzhak[1,*], **Johannes Aberl**[2], **Enrique Prado-Navarrete**[2], **Lada Vukušić**[2], **Agnieszka Anna Corley-Wiciak**[1], **Oliver Skibitzki**[1], **Marvin Hartwig Zoellner**[1], **Markus Andreas Schubert**[1], **Michele Virgilio**[3], **Moritz Brehm**[2], **Giovanni Capellini**[1,4] and **Davide Spirito**[1,5]

[1] IHP—Leibniz-Institut für innovative Mikroelektronik, Im Technologiepark 25, 15236 Frankfurt (Oder), Germany
[2] Institute of Semiconductor and Solid State Physics, Johannes Kepler University Linz, Altenberger Straße 69, 4040 Linz, Austria
[3] Dipartimento di Fisica 'E. Fermi', Università di Pisa, Largo Pontecorvo 3, 56127 Pisa,Italy
[4] Dipartimento di Scienze, Università Roma Tre, V.le G. Marconi 446, 00146 Roma, Italy

E-mail: ryzhak@ihp-microelectronics.com

Received 19 July 2024, revised 10 September 2024
Accepted for publication 25 September 2024
Published 7 October 2024

Abstract
We investigate the nanoheteroepitaxy (NHE) of SiGe and Ge quantum dots (QDs) grown on nanotips (NTs) substrates realized in Si(001) wafers. Due to the lattice strain compliance, enabled by the nanometric size of the tip and the limited dot/substrate interface area, which helps to reduce dot/substrate interdiffusion, the strain and SiGe composition in the QDs could be decoupled. This demonstrates a key advantage of the NHE over the Stranski–Krastanow growth mechanism. Nearly semi-spherical, defect-free, ∼100 nm wide SiGe QDs with different Ge contents were successfully grown on the NTs with high selectivity and size uniformity. On the dots, thin dielectric capping layers were deposited, improving the optical properties by the passivation of surface states. Intense photoluminescence was measured from all samples investigated with emission energy, intensity, and spectral linewidth dependent on the SiGe composition of the QDs and the different capping layers. Radiative recombination occurs in the QDs, and its energy matches the results of band-structure calculations that consider strain compliance between the QD and the tip. The NTs arrangement and the selective growth of QDs allow to studying the PL emission from only 3–4 QDs, demonstrating a bright emission and the possibility of selective addressing. These findings will support the design of optoelectronic devices based on CMOS-compatible emitters.

Supplementary material for this article is available online

Keywords: SiGe, Ge, quantum dot, nanoheteroepitaxy, MBE, micro-photoluminescence, optical coating

[5] Current address: BCMaterials, Basque Center for Materials, Applications and Nanostructures, UPV/EHU Science Park, 48940 Leioa, Spain
[*] Author to whom any correspondence should be addressed.

1. Introduction

In recent years, quantum dot (QDs) devices have been vastly studied due to their unique optical properties [1] for applications such as lasers, light-emitting diodes, single-photon emitters, solar cells, and sensors [2, 3]. In silicon (Si), the workhorse material for the electronic industry, light emission is limited to cryogenic temperatures due to its indirect bandgap. Efficient and practical solutions for Si-based room-temperature (RT) light emission and lasing have been a significant challenge in the field of photonics. Strategies to improve the emission include alloying Si with Ge [4, 5], changing the crystal structure [6], applying strain [7] and applying quantum confinement [8]. Thereby, SiGe QDs offer a tuning knob to steer the emission wavelength to the desired wavelengths by control of bandgap and quantum confinement, achieved by constructing an appropriate heterostack structure [4]. Other alternatives are alloys with Sn in binary GeSn or ternary SiGeSn heteroepitaxy and microstructures, such as microdisks [9].

For example, one recent improvement in RT emission from Si is based on small Ge QDs grown directly on Si substrates co-implanted by low-energy Ge ions [10, 11] which leads to the formation of specific defects (Ge split-[110] self-interstitials (SSI)) within the QDs [12, 13]. These defect-enhanced Ge quantum dots (DEQDs) show pronounced photoluminescence (PL) [10–12, 14], electroluminescence (EL) emission even at 100 °C [15] and evidence of lasing [10]. Theoretical predictions based on ab initio calculations highlight that the SSI defect opens up a recombination path in Ge and SiGe that is optically direct in k-space [12, 13, 16, 17].

However, all previous calculations on SSIs in Ge [12, 13, 16], were performed using an unstrained and pure Ge crystal. That stands heavily in contrast to what is typically observed experimentally for the Stranski–Krastanow (SK) growth of Ge on Si QDs [18]. The formation of QDs on a ∼0.5 nm monolayer thick Ge-rich wetting layer is primarily governed by the lattice mismatch between the Si and Ge [19–21] of 4.2%. The heteroepitaxial strain is also partially accommodated by the SiGe intermixing occurring even when Ge layers are deposited on Si at low epitaxial growth temperatures [22, 23], and by QDs, such as hut clusters [24], used to create DEQDs. Furthermore, the nucleation of QDs on planar substrates is stochastic [25], leading to variations in QD size [26], chemical uniformity [27] and spacing, ultimately limiting their addressability. Nucleation site control of QDs and slight improvement of the alloy composition uniformity of the QDs can be achieved by substrate pre-patterning [28, 29] or strain modulation [30].

Thus, there is an evident need to create an experimental model platform on a Si substrate that combines (i) a low-strain environment, (ii) confinement of charge carriers in QDs, and (iii) the possibility of tuning the SiGe alloy concentration in the QD. Site-selectivity of the nanostructures, achievable for SK QDs only via elaborated substrate pre-patterning techniques, would be preferential as it allows for mandatory device addressability. Importantly, capping strategies need to be developed for an unstrained SiGe QD platform to limit non-radiative emission from surface states and to potentially allow for post-growth *ex-situ* implantation of the nanostructures to introduce the beneficial DEQD defects.

Here, we developed a platform for nearly strain-free SiGe QDs, grown epitaxially on Si(001) nanotip (NT) patterned substrates. We used the nanoheteroepitaxy (NHE) approach to improve the structural quality of the grown QDs. NHE [31–33] is the epitaxial growth on small crystalline areas on an else amorphous substrate, and has been successfully used in various material systems such as InP/Si [34], Ge/Si [35], GaAs/Si and GaP/Si [36, 37]. It takes advantage of small interfaces between QD and NT, reducing the intermixing during growth and annealing. Furthermore, the two materials are only connected at the nanoscale level, which prevents substrate cracking or bowing due to the mismatch in the thermal expansion coefficient between the different materials. The NHE concept [38] is based on the compliance effect, i.e. the distribution of strain between QD material and Si NT to overcome the significant lattice mismatch. Moreover, the deterministic site control of SiGe QDs of various compositions presented here significantly improves their accessibility and feasibility for future integrated technologies. Our approach allows for an efficient decoupling of strain and SiGe composition in the QDs, which is different from conventional SK QDs, while enabling QD size, shape, position, and density control. An additional thin layer of Si_3N_4, Al_2O_3 or Si was deposited on the QDs, to investigate the role of capping on their structure and optical properties. Following QDs characterization, we will examine the QDs structural and optical properties, evaluating their potential to semiconductor technology.

2. Methods

NT-patterned Si-(001) substrates were manufactured using a state-of-the-art 0.13 μm SiGe BiCMOS technology pilot line on 200 mm wafers. As the last production steps, free-standing 800 nm high Si NTs were first covered in silicon dioxide (SiO_2) using plasma-enhanced chemical vapor deposition and afterwards the surface was polished using chemical mechanical planarization, defining hereby the Si NT top opening diameter in the range of 50–90 nm. Details of the substrate fabrication can be found in [39, 40]. The NTs were arranged in arrays with an inter-tip spacing of 0.5 μm, 0.8 μm, 1 μm and 2 μm, with the primary focus of our study being on the 0.5 μm pitch size.

The deposition of Ge and SiGe QDs on top of the Si NTs was performed using solid-source molecular beam epitaxy (SSMBE). Growth rates and deposition temperature are decoupled during the Ge MBE process. This is essential to achieve prototype site-controlled Ge and SiGe QDs on NT-patterned substrates with excellent crystalline quality [39].

Before the QD growth, chips 22 mm $\times$ 22 mm in size were cut from the 200 mm Si NT substrate and cleaned using a combination of Piranha etch and RCA wet-chemical cleanings, followed by a dip in diluted hydrofluoric acid (10 sec) at the end of the cleaning process [39] to remove native Si oxide at the NT surface. After loading the substrates into the SSMBE growth chamber, the chips were degassed and pre-annealed for 20 min at 790 °C. A series of samples were grown by deposition of an equivalent thickness of 10 nm SiGe with Ge content of 50%, 78.3%, and 100% without capping. The pure Ge sample was grown at a temperature of 750 °C, mimicking the results of [39]. However, for the deposition of SiGe alloys, the growth temperature needed to be raised to 850 °C to ensure perfectly site-controlled QDs growth. Another series of samples were prepared with 40 nm equivalent thickness of pure Ge QDs. These were subsequently capped with (i) $\sim$1.5 nm of Si, deposited at 350 °C in the SSMBE system, (ii) $\sim$10 nm of Al_2O_3 externally deposited by atomic layer deposition, or (iii) with $\sim$40 nm of Si_3N_4 using a physical vapor deposition system.

Atomic force microscopy (AFM) images were recorded using a Dimension 3100 from Veeco. Energy dispersive x-ray spectroscopy (EDX) measurements were performed using a FEI Tecnai Osiris operated at 200 kV in scanning transmission electron microscopy mode. Samples for TEM were prepared using the conventional method of grinding, polishing, and Argon ion thinning. X-ray-diffraction (XRD) was conducted with a Rigaku SmartLab tool featuring a 9 kW rotating Cu-Anode. It was set to high-resolution double crystal diffraction using a Ge(400)x2 channel cut monochromator. The (004) and (224) Bragg reflections were scanned to receive the in-plane and out-of-plane lattice spacings of the Ge QDs and calculate the lattice constant a_{Ge} via a biaxial strain model and the Poisson ratio ($\nu_{\mathrm{Ge}} = 0.273$) [41] and the corresponding in-plane ($\varepsilon_{\|}$), out-of-plane ($\varepsilon_{\perp}$) as well as hydrostatic strain (ε_{V}) in reference to the Ge lattice constant ($a_0 = 5.6575$ Å).

Micro-photoluminescence (μ-PL) measurements were performed with a HORIBA iHR 320 spectrometer equipped with a Synapse/Symphony InGaAs II detector, 50x objective with $\sim$1 μm spot size. We used a grating with 600 grooves/mm, which covers a wavelength range from 1000 to 2000 nm with a spectral resolution of 0.06 nm, with an excitation laser at 532 nm wavelength. The temperature dependence was determined using a LN_2–cooled cryostat and an excitation power of 11.3 mW (2×10^6 W cm^{-2}). We collected all the spectra in backscattering geometry and used a white lamp to calibrate the setup spectral response. All PL spectra were analyzed as a single Gaussian peak.

To account for alloying and strain induced effects, bulk-like band edge energies in the valence and conduction bands have been calculated in the framework of the model solid theory [42] for different degrees of strain relaxation in the QD. To this aim, the deformation potentials of SiGe have been estimated as linear interpolation of the corresponding Si and Ge values. Modification of the energy levels in the QD induced by quantum confinement effects are expected to be negligible due to the relatively large size of the dots and hence have been neglected.

3. Results and discussion

3.1. Structural quality and μ-photoluminescence of the uncapped samples

In figures 1(a)–(c) we show the AFM images of SiGe QDs arrays with Ge concentration 100%, 78% and 50%, without capping. The selection of these specific concentrations is likely exemplary to cover a range of Ge-Si interactions and to understand the transition from Ge-dominant to Si-dominant behaviors. The QDs grow at the NT's position, and for all the QDs compositions, the growth is almost completely selective on the Si NT exposed area, with a negligible density of nucleation events occurring on the SiO_2 mask.

Figure 2 shows TEM images for the sample with 50% Ge content. The selective growth of the QDs on the Si NTs is evident (figure 2), with high-quality, nearly defect-free nanostructures. Panel (a) of figure 2 demonstrates the consistency of SiGe QDs. The subsequent images at higher magnifications (panels (b)–(d)) illustrate the high quality of the crystals. Indeed, the well-controlled growth processes and parameters have resulted in almost semi-spherical SiGe QDs deposited evenly and entirely over Si NTs. Also, in principle, the presence of defects, such as stacking faults (SFs) and dislocations, in SiGe QDs on Si NT can cause strain relaxation and a reduction in the quantum confinement [43] effect, leading to changes in the electronic and optical properties [44]. However, TEM investigations from these samples did not show the presence of extended defects in these QDs. The possibility of 3D growth with limited influence of the substrate allows for an optimal strain relaxation, slightly dependent on the composition, as will be discussed in the following.

Another critical parameter is the growth temperature of SiGe QDs, which significantly influences the selectivity and structural properties. Higher growth temperatures favor the selective growth of SiGe QDs within specific regions, such as Si NT. Lower temperatures, on the other hand, may result in less selectivity and a random distribution of QDs on the substrate surface. For the deposition of pure Ge on NT substrates, a substrate growth temperature of 750 °C allows for sufficient surface mobility of the Ge ad-atoms for perfect site-controlled growth. However, the addition of Si and the hence reduced surface kinetics leads to the nucleation of surface clusters at the entire substrate surfaces, as can be seen in the AFM image figure S1 in the supplementary material. Growth temperatures of 750 °C were tested for the deposition of $Si_{0.1}Ge_{0.9}$ QDs. Even though only 10% of Si was added to the Ge, the presence of Si leads to non-site-selective cluster formation at the entire substrate surface. An increase in the growth temperature of only 100 °C allows for the fabrication of SiGe QDs over a wide composition range of the SiGe alloy, see, e.g. figure 2 for $Si_{0.5}Ge_{0.5}$.

A detailed analysis of the QD shape was obtained with cross-section TEM, shown in figures 3 (a) and (b). The TEM images highlight that the QDs grow on the tip surface and assume a 3D shape. This shape is determined by several factors: the interface energy at the Si NT, surface energy, and the internal elastic energy caused by strain [45]. All these

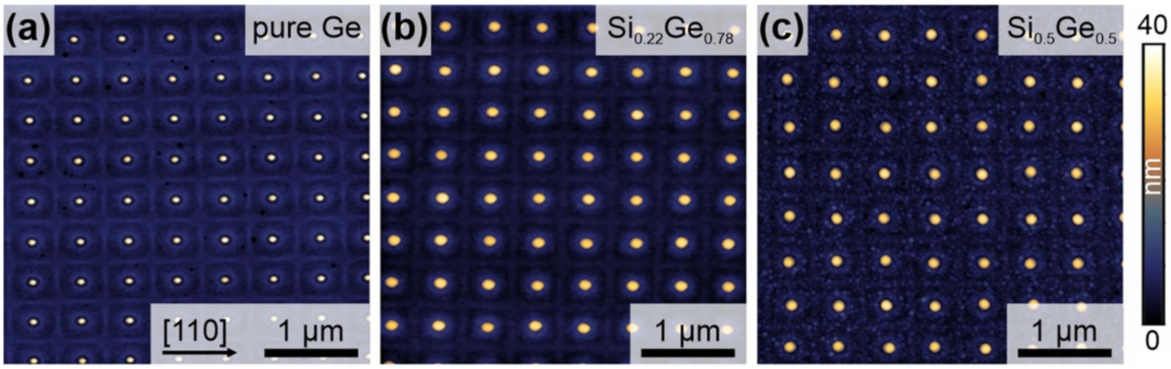

Figure 1. (a)-(c) AFM topography of Ge and SiGe QDs grown on substrates with a NT pitch of 500 nm. The Ge concentration 100%, 78% and 50%.

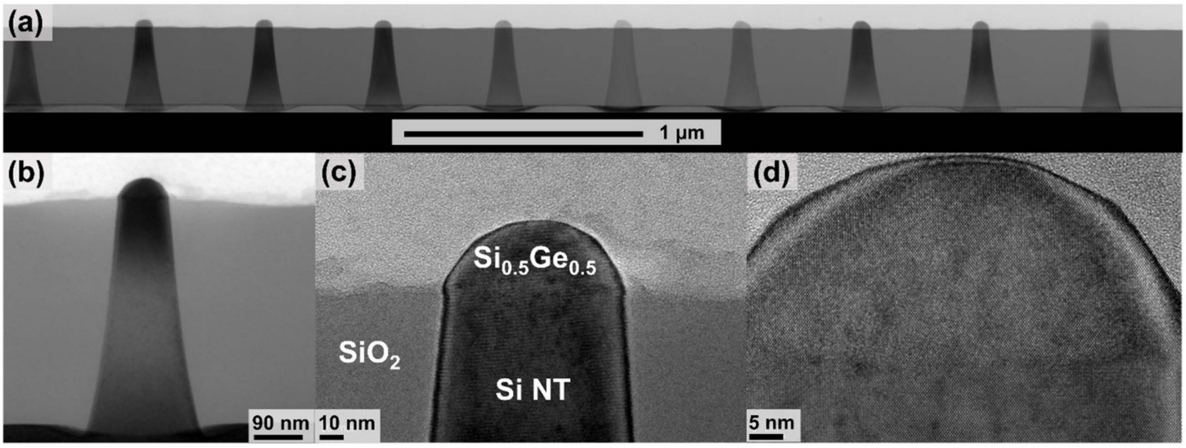

Figure 2. Cross-section TEM at different magnification for $Si_{0.5}Ge_{0.5}$ QDs on Si NTs with pitch size of 0.5 μm.

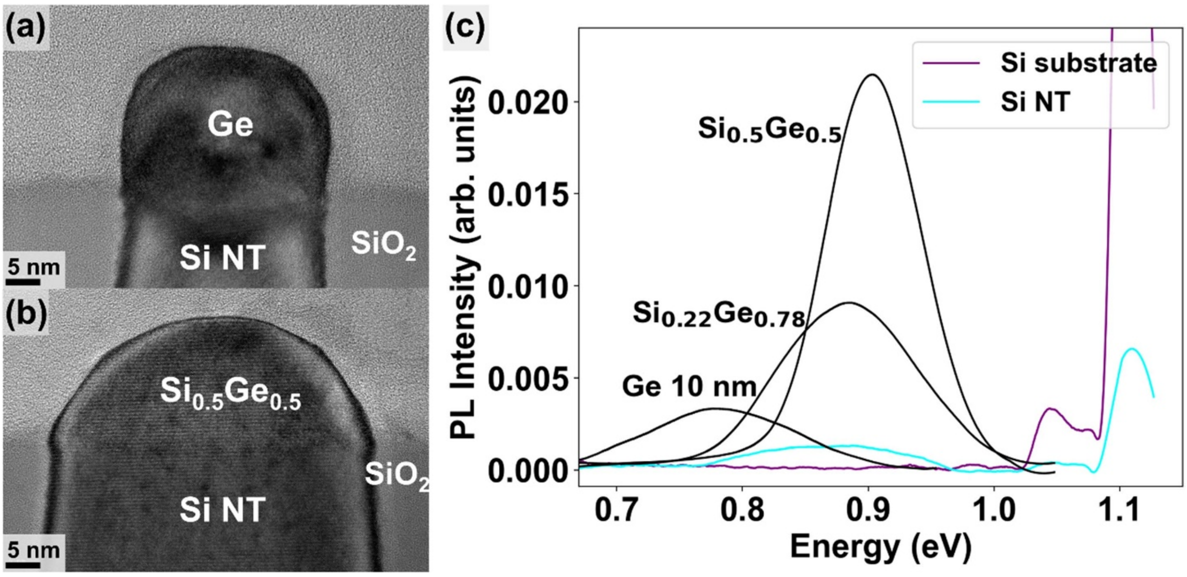

Figure 3. TEM of QDs (10 nm equivalent thickness) on Si NTs with varying Ge concentrations. (a) Ge (b) $Si_{0.5}Ge_{0.5}$ alloy. (c) μ-PL spectra at temperature of 80 K.

parameters depend on the alloy composition, amount of material in the QD, and deposition conditions. In our case, we observe that an uncapped pure Ge QD (figure 3(a)) forms rounded shapes [46], as surface energy is high, which typically minimizes the surface area to volume ratio. The Ge QDs shape indicates that the surface energy is not significantly anisotropic and that the strain within the QD mostly is uniformly distributed, allowing a rounded morphology.

The internal strain within the SiGe 50%, in figure 3(b), seems to be lower than at higher Ge contents, leading to a shape that is more influenced by the interface strain with the Si NT. The surface energy could promote growth in specific directions, resulting in a more defined and elongated structure. The semi-spherical shape of the SiGe QDs is primarily the result of the surface tension during the growth process, which naturally leads to a shape that minimizes the surface energy [47]. This effect, combined with the lattice mismatch between the SiGe, guides the atoms to arrange into smooth, semi-spherical structures to reduce the overall system energy [48].

SK-grown QDs are more strained when their shape is more rounded and more relaxed with a semi-spherical shape [49]. The rounded shape of our patterned Ge QDs structure leads to symmetric strain distribution [50], minimizing variations in stress along different directions. The semi-spherical QDs shaped composed of 50% Ge and 50% Si may exhibit more significant variations in its bandgap due to a 2% lattice mismatch. The bandgap energy of these QDs is likely to be intermediate between pure Si and pure Ge [51].

The electronic states were investigated through μ-PL spectroscopy at 80 K, as displayed in the spectra in figure 3(c), for the uncapped SiGe QDs of various nominal SiGe alloy composition as well as for bare Si NT and Si substrate as reference. We can consider that the emission derives only from those QDs illuminated by the laser, as the structure with NTs and SiO_2 matrix reduced the diffusion of photoexcited carriers. Thus, considering the spot size of the μ-PL setup (diameter $\sim$1 μm) and the pitch of the QD array under investigation (0.5 μm), we can assume that the measured emission came from 3–4 QDs.

We observed one single PL peak for each sample, with an approximately Gaussian line shape. The peak shifts with increasing Si alloy composition from $\sim$0.78 eV to $\sim$0.9 eV. Bare Si NT had a weak emission at 0.855 eV, corresponding to the spectral fingerprint of D1 dislocations in Si [52]. This emission is likely a consequence of the Si NTs fabrication process. This monotonous blue shift of the PL emission from the QDs with increasing Si content in the SiGe alloy indicates that the PL origin is related to the SiGe QDs. The energy of the PL emission observed in SiGe QDs can be attributed to the combined effects of alloy composition and strain. The smallest full-width at half maximum (FWHM) is 85 meV for QDs of $Si_{0.5}Ge_{0.5}$, and the FWHM becomes larger (150 meV) for Ge_{100}. The fact that the peak is the narrowest in the $Si_{0.5}Ge_{0.5}$ QDs suggests that these QDs are in the optimal condition to reduce the non-radiative transition. This finding also suggests the potential importance of further reducing non-radiative mechanisms, possibly through enhanced coating techniques or post-growth processing. Another approach could be to reduce the size of the QDs, which would enhance quantum confinement.

SiGe heterostructures can feature either a band alignment of type-I (both holes and electrons are confined in the same layer of the heterostructure) or type-II (electron and holes confined in the two different sides of an heterojunction), depending on the composition and strain of both layers [53]. It has been proven that Ge-rich nanostructures on Si show type-II alignment with a large valence band offset that confines holes in the Ge layer and a very moderated conduction band offset that favors accumulation of electrons in the Si side [54, 55]. Here, we deal with strain-relaxed nanostructures resulting from the distribution of strain between the QD and the NT. To estimate the band edge in the QD, we consider this compliance effect assuming a distribution of biaxial strain along the interface in same proportion between QD and NT. We ignore the complex modeling of the spatial variation of the strain in the QD. Quantum confinement can also be ignored considering the size of the QD, since the Bohr radius for excitons in Ge around 25 nm [56], smaller than the size of the QDs in this study. The dominant transition at all the composition is assigned to Δ_4 valley in conduction band and heavy hole valence band of the QDs. In pure Ge, we note that Δ_4 and L valleys are almost degenerate, but Δ_4 is lower in energy due to the strain (see also table S1 in supplementary materials).

The simulated emission energy matches approximatively with the experimental values, and assume a shift of $\sim$170 meV between Ge and $Si_{0.5}Ge_{0.5}$, compared with a value of $\sim$120 meV from the experiment. Broadening of the spectra can occur because of reduced recombination lifetime, or because of a spreading of the transition energy associated with spatial strain distribution. The uniformity of QDs and the limited number of them that participate to the emission limits the statistical spread. Additionally, broadening can be due to splitting of the valence band or to phonon replica of the main peak. When analyzed in details Ge QDs (figure S2), the PL spectra present a shoulder at lower energy and with a small separation from the main peak, about 60 meV apart. In [55], a splitting of about 56 meV (close to our 60 meV) is associated with transitions involving the emission and absorption of an optical phonon with energy $E = 28$ meV.

3.2. QDs capping

For optical application, the nanostructures must be capped to passivate surface states that can act as non-radiative recombination centers. As a proof of principle, we tested different capping layer materials on pure Ge QDs (40 nm thickness) on Si NTs. Figures 4(a)–(d) presents TEM images of uncapped Ge QDs on NT, and capped Ge QDs with Si, Si_3N_4 and Al_2O_3, respectively (figures 4(b)–(d)). The elemental distribution obtained from TEM/EDX analysis (figures 4(e)-(h)) provides additional insight. First, it confirms that the growth is highly selective also for this amount of deposited Ge. Second, we observe Ge growth around Si-NT top, which can be assigned as Si NT SFs that form around the SiO_2 'wall' [57, 58], which was seen in our previous studies [59]. Using XRD, we measured a compressive strain for all the capped samples in the range of -0.1% to -0.3% (supplementary material, figure S3). The magnitude of the strain depends on the capping material. We note that such low strain for pure Ge on Si nanostructures represents a substantial deviation from the typical high-strain environment in SK QDs.

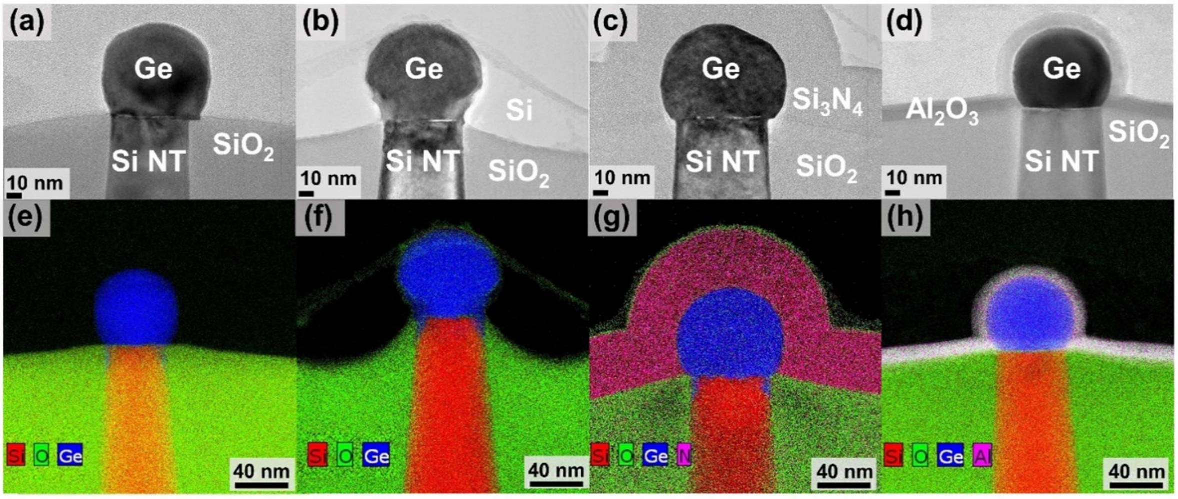

Figure 4. TEM and EDX images of cross-section Ge QDs on Si NT: (a) and (e) without capping; (b) and (f) Si cap; (c) and (g) Si_3N_4 cap; (d) and (h) Al_2O_3 cap. In the EDX maps, colors are assigned to elements as Ge (blue), Si (red), O (green) and pink color with capping (Si; Si_3N_4; Al_2O_3).

Typically, Ge SK QDs can be successfully capped with Si due to the limited strain relaxation occurring in the QD. The thickness of the Si layer also plays a critical role, potentially altering their shape from pyramids to domes [60]. Depending on the thickness and conditions of deposition (i.e. temperature), Si capping can either compress or stretch the underlying Ge dot [61]. As the Si cap thickness increases, the cap can partially relax by forming its strain gradient that counteracts the expansion due to the SiGe dots, which impacts the electronic properties by modifying the band structure [62]. Our NHE approach used controlled interfaces between QDs and NTs and provided distinct capping behaviors. This does not only preserve the structural integrity of the QDs but also enhances their properties by reducing mismatch in the coefficient of thermal expansion that is common in traditional capping methods.

For the here presented SiGe NTs, Si might not be the best choice as a capping material since the high strain contrast between relaxed SiGe QDs and the hence highly tensile strained Si capping layer leads to pronounced dislocation formation (supplementary material, figure S4). Applying thin but tensile-strained Si capping layers lead to challenges in achieving even a conformal overgrowth of the Ge QDs, as intermixing and growth around Si NT issues are evident in figures 4(b) and (f). In addition, the SiO_2 structures appear more vulnerable to degradation when they come into contact with the Si capping layer. Si in the capping layer reacts with the SiO_2 mask under the growth conditions. In this way, the mask is partially etched in the region not shaded by the QD, as seen in figure 4(a).

We used post-growth deposited Al_2O_3 and Si_3N_4 as capping material to circumvent this strain misfit on our Ge pure 40 nm QDs. In contrast to Si capping, using a Si_3N_4 capping layer seems a good choice, as it provides a conformal growth around the QD, as evidenced by the EDX image in figure 4(g). Al_2O_3 appears thinner on the QD than on the substrate figure 4(h). We observe that the presence of Si_3N_4 provides a stable, chemically inert environment that prevents the Si from diffusing into other layers and allows for a more controlled and uniform capping layer growth while conserving the QD shape.

As we mentioned before, in contrast to conventional SK QDs, the residual strain in the QDs is close to zero. For the capped samples, the magnitude of the strain depends on the capping material and is for all samples in the range of -0.1% to -0.3%. Consequently, the PL emission is expected to shift to higher energy with respect to the uncapped case. In figure S3 of the supplementary material, we additionally report the energy as a function of the measured strain. Figure 5(a) depicts the PL spectra obtained from Ge_{100} QDs with different capping layers. Notably, we found that the Al_2O_3 and the Si_3N_4 capping layers improved the intensity of the PL emission. This improvement can be associated with a suppression of the non-radiative recombination due to surface states. Also, the smallest FWHM (90 meV) for Al_2O_3 and Si_3N_4 indicates that those capping layers enable good surface passivation.

The integrated PL intensity (figure 5(b)) as a function of power follows a power law as $I_{PL} \propto P^{m}$ [63]. Based on experimental data, the exponent m is in the range of 0.83–1.2 (supplementary material, table S1), Si_3N_4 having has $m = 0.83$. The value of the exponent m is the result of the interplay of radiative recombination, non-radiative recombination via defects, and the Auger effect [64]. When $m \sim 1$, the effect of defects is relevant in comparison with band-to-band recombination, but defect states can be considered as not saturated. This usually occurs at low excitation power; high pump power result in saturation of defect energy level, leading to $m \sim 1/2$ [63]. Auger recombination [65, 66] is a non-radiative process, in which the energy released by the recombination of an electron and a hole is transferred to a third carrier, instead of being

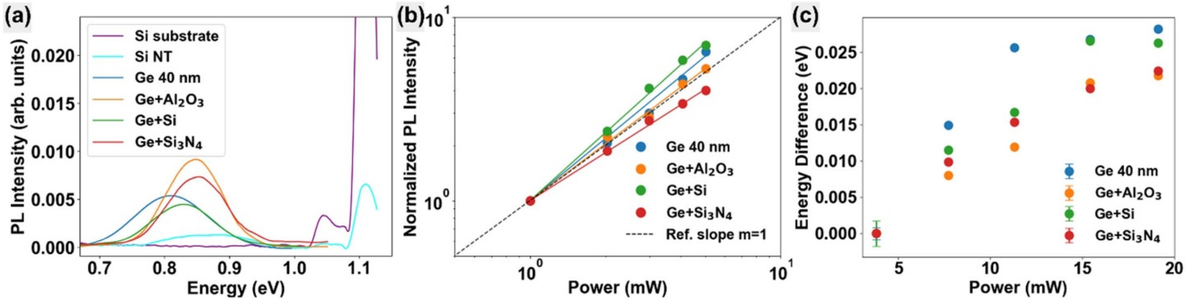

Figure 5. (a) μ-PL spectra at temperature of 80 K of Ge QDs with capping layers. Reference signals of the Si substrate and the Si NT are indicated in violet and light blue. (b) PL intensity normalized to the minimum power as a function of the excitation power for uncapped and differently capped Ge QDs with dashed black dashed line as a ref. slope m = 1. (c) Main peak energy as a function of excitation power, reported with reference to the minimum power.

emitted as a photon, and has a dependence on the photoexcited carrier density with $m \sim 2/3$, thus becomes relevant at high power.

Surface passivation [67] using capping layers such as Al_2O_3 and Si_3N_4 [68] effectively reduces surface states that serve as non-radiative recombination centers. One of the methods for surface passivation is chemical passivation, which involves reducing defect density by depositing a capping layer. This layer chemically bonds with the Ge dangling bonds, creating a stable interface, thus decreasing the number of recombination centers [69]. Another mechanism is associated to charged defects in the Si_3N_4 films, that usually contain a high density of positive charges [68]. These charges can create an electric field at the Ge surface [68], repelling minority carriers and thus reducing surface recombination. This reduction leads to a decrease in overall non-radiative recombination, including Auger recombination. The low power law exponent ($m = 0.83$) observed with Si_3N_4 capping indicates that this material provides the most effective passivation for our Ge QDs.

The power dependence of PL emission energy [70] can tell about density of states (DOS). The shift suggests that there is a either a limited joint DOS for the transition or that recombination is not efficient with respect to excitation [71]. When the excitation power is increased, the peak shift to higher energy due to state-filling. This is specific to zero-dimensional systems like QDs [72], where the discrete DOS results in the population of higher energy states as lower states are filled [72, 73]. One characteristic feature of the state-filling effect is the saturation of lower-energy PL peaks as the excitation intensity increases. Figure 5(c) demonstrates that the energy difference increases with the excitation power for all Ge QDs samples, indicating the state-filling effect in zero-dimensional systems. As the electron density increases, the PL peak position shifts towards higher energy (blueshift). This blueshift indicates that lower energy states are being filled, forcing electrons to occupy higher energy states [72, 74]. However, at higher powers, this increase becomes saturated. This saturation [75] happens while intersubband level carrier relaxation to the lower level slows down under the limited availability of higher/final energy states.

A further indication of the complexity of the energy level in these QDs comes from temperature-dependent PL, that was performed for Ge QDs with and without a capping layer and SiGe QDs (supplementary material, figure S5). As the sample temperature increased, we observed a clear redshift and broadening of the PL spectra, accompanied by a decreased PL intensity. However, the peak position did not follow the Varshni rule, typically observed in bulk Ge [76, 77], as the strain-free QDs on NTs shifted less than expected in the measured temperature range (supplementary material, figure S5). This deviation from the Varshni trend is interesting and suggests that the electronic and optical properties of SiGe QDs may differ from those of bulk Ge. It can be attributed to various factors, including strain compliance between QD and NT, and temperature-induced relevant changes in the strain of the QDs due to the mismatch of thermal expansion and encapsulation of the NTs with SiO_2. In particular, we observed saturation behavior in the energy shift for Ge with different capping layers above 120 K.

4. Conclusions

Based on the NHE approach, we have successfully fabricated virtually strain-free SiGe QDs of various Ge content on Si NTs. Our results demonstrate that we can use the patterned substrate to control the growth dynamics of SiGe alloys beyond the interplay of composition and size that occurs in standard epitaxial growth on unpatterned substrates. The QDs exhibit pronounced optical properties in terms of PL, dependent on the composition and associated to indirect transition in the QD itself. The luminescence emission could be further enhanced by applying various capping layer strategies, for this purpose, the best materials are Al_2O_3 and Si_3N_4. The ability to control the growth dynamics and tailor the properties of SiGe QDs through the NHE approach presents new opportunities for designing and optimizing optoelectronic devices for a wide range of applications. The strain in SiGe QDs on NTs is significantly reduced as compared to conventional SiGe SK QDs on Si, making this system an ideal testbed to study the influence of light-emitting defects in nanoconfined, low-strained SiGe.

Data availability statement

The data that support the findings of this study are available upon reasonable request from the authors.

Acknowledgment

This research was funded in whole or in part by the Austrian Science Fund (FWF) [10.55776/Y1238]. For open access purposes, the author has applied a CC BY public copyright license to any author-accepted manuscript version arising from this submission. Also, funding from the Linz Institute of Technology (LIT): Grant Nos. LIT-2019-7-SEE-114 is kindly acknowledged.

ORCID iDs

Diana Ryzhak https://orcid.org/0009-0007-4941-7383
Johannes Aberl https://orcid.org/0000-0002-2308-7538
Enrique Prado-Navarrete https://orcid.org/0000-0002-8233-6979
Lada Vukušić https://orcid.org/0000-0003-2424-8636
Oliver Skibitzki https://orcid.org/0000-0001-5582-5008
Marvin Hartwig Zoellner https://orcid.org/0000-0001-7204-1096
Michele Virgilio https://orcid.org/0000-0002-7847-6813
Moritz Brehm https://orcid.org/0000-0002-5629-5923
Giovanni Capellini https://orcid.org/0000-0002-5169-2823
Davide Spirito https://orcid.org/0000-0002-6074-957X

References

[1] Agarwal K, Rai H and Mondal S 2023 Quantum dots: an overview of synthesis, properties, and applications *Mater. Res. Express.* **10** 062001
[2] Masumoto Y and Takagahara T 2011 *Semiconductor Quantum Dots: Physics, Spectroscopy and Applications* (Springer)
[3] Basu R and Singh A 2021 High temperature Si–Ge alloy towards thermoelectric applications: a comprehensive review *Mater. Today Phys.* **21** 100468
[4] Tsybeskov L and Lockwood D J 2009 Silicon-germanium nanostructures for light emitters and on-chip optical interconnects *Proc. IEEE* **97** 1284–303
[5] Fischer I A, Brehm M, De Seta M, Isella G, Paul D J, Virgilio M and Capellini G 2022 On-chip infrared photonics with Si-Ge-heterostructures: what is next? *APL Photonics* **7** 050901
[6] Fadaly E M T *et al* 2020 Direct-bandgap emission from hexagonal Ge and SiGe alloys *Nature* **580** 205–9
[7] Corley-Wiciak C *et al* 2023 Nanoscale mapping of the 3D strain tensor in a germanium quantum well hosting a functional spin qubit device *ACS Appl. Mater. Interfaces* **15** 3119–30
[8] Barbagiovanni E G, Lockwood D J, Simpson P J and Goncharova L V 2014 Quantum confinement in Si and Ge nanostructures: theory and experiment *Appl. Phys. Rev.* **1** 011302
[9] Buca D *et al* 2022 Room temperature lasing in GeSn microdisks enabled by strain engineering *Adv. Opt. Mater.* **10** 2201024
[10] Grydlik M, Hackl F, Groiss H, Glaser M, Halilovic A, Fromherz T, Jantsch W, Schäffler F and Brehm M 2016 Lasing from glassy Ge quantum dots in crystalline Si *ACS Photonics* **3** 298–303
[11] Spindlberger L, Kim M, Aberl J, Fromherz T, Schäffler F, Fournel F, Hartmann J-M, Hallam B and Brehm M 2021 Advanced hydrogenation process applied on Ge on Si quantum dots for enhanced light emission *Appl. Phys. Lett.* **118** 083104
[12] Grydlik M, Lusk M T, Hackl F, Polimeni A, Fromherz T, Jantsch W, Schäffler F and Brehm M 2016 Laser level scheme of self-interstitials in epitaxial Ge dots encapsulated in Si *Nano Lett.* **16** 6802–7
[13] Murphy-Armando F, Brehm M, Steindl P, Lusk M T, Fromherz T, Schwarz K and Blaha P 2021 Light emission from direct band gap germanium containing split-interstitial defects *Phys. Rev.* B **103** 085310
[14] Zinovieva A F, Zinovyev V A, Nenashev A V, Teys S A, Dvurechenskii A V, Borodavchenko O M, Zhivulko V D and Mudryi A V 2020 Photoluminescence of compact GeSi quantum dot groups with increased probability of finding an electron in Ge *Sci. Rep.* **10** 9308
[15] Rauter P, Spindlberger L, Schäffler F, Fromherz T, Freund J and Brehm M 2018 Room-temperature group-IV LED based on defect-enhanced Ge quantum dots *ACS Photonics* **5** 431–8
[16] Moreira M D, Miwa R H and Venezuela P 2004 Electronic and structural properties of germanium self-interstitials *Phys. Rev.* B **70** 115215
[17] Spindlberger L, Aberl J, Vukušić L, Fromherz T, Hartmann J-M, Fournel F, Prucnal S, Murphy-Armando F and Brehm M 2024 Light emission from ion-implanted SiGe quantum dots grown on Si substrates *Mater. Sci Semicond. Process.* **181** 108616
[18] Wiebach T, Schmidbauer M, Hanke M, Raidt H, Köhler R and Wawra H 2000 Strain and composition in SiGe nanoscale islands studied by x-ray scattering *Phys. Rev.* B **61** 5571–8
[19] Seta M D, Capellini G, Evangelisti F and Spinella C 2002 Intermixing-promoted scaling of Ge/Si(100) island sizes *J. Appl. Phys.* **92** 6149
[20] Capellini G, De Seta M and Evangelisti F 2001 SiGe intermixing in Ge/Si(100) islands *Appl. Phys. Lett.* **78** 303–5
[21] Aberl J, Brehm M, Fromherz T, Schuster J, Frigerio J and Rauter P 2019 SiGe quantum well infrared photodetectors on strained-silicon-on-insulator *Opt. Express* **27** 32009
[22] Mastari M 2019 Growth and characterization of SiGe alloys on nanometer-size structures for microelectronics applications *Theses* University Grenoble Alpes
[23] Brehm M and Grydlik M 2017 Site-controlled and advanced epitaxial Ge/Si quantum dots: fabrication, properties, and applications *Nanotechnology* **28** 392001
[24] Zinovyev V A, Zinovieva A F, Nenashev A V, Dvurechenskii A V, Katsuba A V, Borodavchenko O M, Zhivulko V D and Mudryi A V 2020 Self-assembled epitaxial metal–semiconductor nanostructures with enhanced GeSi quantum dot luminescence *J. Appl. Phys.* **127** 243108
[25] Capellini G, Seta M D and Evangelisti F 2003 Ge/Si(100) islands: growth dynamics versus growth rate *J. Appl. Phys.* **93** 291–5
[26] Wen W-C, Schubert M A, Zoellner M H, Tillack B and Yamamoto Y 2023 Three-dimensional self-ordered multilayered Ge nanodots on SiGe *ECS J. Solid State Sci. Technol.* **12** 055001
[27] Grützmacher D *et al* 2007 Three-dimensional Si/Ge quantum dot crystals *Nano Lett.* **7** 3150–6
[28] Pezzoli F, Stoffel M, Merdzhanova T, Rastelli A and Schmidt O 2009 Alloying and strain relaxation in SiGe

islands grown on pit-patterned Si(001) substrates probed by nanotomography *Nanoscale Res. Lett.* **4** 1073
[29] Brehm M, Grydlik M, Hackl F, Lausecker E, Fromherz T and Bauer G 2010 Excitation intensity driven PL shifts of SiGe islands on patterned and planar Si(001) substrates: evidence for Ge-rich dots in islands *Nanoscale Res. Lett.* **5** 1868–72
[30] Marchetti R, Montalenti F, Miglio L, Capellini G, De Seta M and Evangelisti F 2005 Strain-induced ordering of small Ge islands in clusters at the surface of multilayered Si–Ge nanostructures *Appl. Phys. Lett.* **87** 261919
[31] Yamamoto Y, Wen W-C and Tillack B 2023 Heteroepitaxy of group IV materials for future device application *Jpn. J. Appl. Phys.* **62** SC0805
[32] Mastari M *et al* 2018 SiGe nano-heteroepitaxy on Si and SiGe nano-pillars *Nanotechnology* **29** 275702
[33] Zaumseil P, Yamamoto Y, Schubert M A, Capellini G, Skibitzki O, Zoellner M H and Schroeder T 2015 Tailoring the strain in Si nano-structures for defect-free epitaxial Ge over growth *Nanotechnology* **26** 355707
[34] Kamath A, Ryzhak D, Rodrigues A, Kafi N, Golz C, Spirito D, Skibitzki O, Persichetti L, Schmidbauer M and Hatami F 2024 Controlled integration of InP nanoislands with CMOS-compatible Si using nanoheteroepitaxy approach *Mater. Sci. Semicond. Process.* **182** 108585
[35] Niu G *et al* 2016 Selective epitaxy of InP on Si and rectification in graphene/InP/Si hybrid structure *ACS Appl. Mater. Interfaces* **8** 26948–55
[36] Kozak R, Prieto I, Arroyo Rojas Dasilva Y, Erni R, Skibitzki O, Capellini G, Schroeder T, von Känel H and Rossell M D 2017 Strain relaxation in epitaxial GaAs/Si (0 0 1) nanostructures *Phil. Mag.* **97** 2845–57
[37] Kafi N *et al* 2024 Selective growth of GaP crystals on CMOS-compatible Si nanotip wafers by gas source molecular beam epitaxy *Cryst. Growth Des.* **24** 2724–33
[38] Schlykow V *et al* 2016 Selective growth of fully relaxed GeSn nano-islands by nanoheteroepitaxy on patterned Si(001) *Appl. Phys. Lett.* **109** 202102
[39] Niu G *et al* 2016 Photodetection in hybrid single-layer graphene/fully coherent germanium island nanostructures selectively grown on silicon nanotip patterns *ACS Appl. Mater. Interfaces* **8** 2017–26
[40] Skibitzki O, Prieto I, Kozak R, Capellini G, Zaumseil P, Arroyo Rojas Dasilva Y, Rossell M D, Erni R, von Känel H and Schroeder T 2017 Structural and optical characterization of GaAs nano-crystals selectively grown on Si nano-tips by MOVPE *Nanotechnology* **28** 135301
[41] Wortman J J and Evans R A 1965 Young's modulus, shear modulus, and poisson's ratio in silicon and germanium *J. Appl. Phys.* **36** 153–6
[42] De Walle C G V 1989 Band lineups and deformation potentials in the model-solid theory *Phys. Rev.* B **39** 1871–83
[43] Ji Z-M, Luo J-W and Li -S-S 2020 Interface-engineering enhanced light emission from Si/Ge quantum dots *New J. Phys.* **22** 093037
[44] Montanari M *et al* 2018 Photoluminescence study of interband transitions in few-layer, pseudomorphic, and strain-unbalanced Ge/GeSi multiple quantum wells *Phys. Rev.* B **98** 195310
[45] Stekolnikov A A and Bechstedt F 2005 Shape of free and constrained group-IV crystallites: influence of surface energies *Phys. Rev.* B **72** 125326
[46] Hong P-Y, Lin C-H, Wang I-H, Chiu Y-J, Lee B-J, Kao J-C, Huang C-H, Lin H-C, George T and Li P-W 2023 The amazing world of self-organized Ge quantum dots for Si photonics on SiN platforms *Appl. Phys.* A **129** 126
[47] Stanchu H *et al* 2024 Comprehensive material study of Ge grown by aspect ratio trapping on Si substrate *J. Phys. Appl. Phys.* **57** 255107
[48] Li X L, Wang C X and Yang G W 2014 Thermodynamic theory of growth of nanostructures *Prog. Mater. Sci.* **64** 121–99
[49] Shahzadeh M and Sabaeian M 2014 A comparison between semi-spheroid- and dome-shaped quantum dots coupled to wetting layer *AIP Adv.* **4** 067134
[50] Yang X-F, Chen X-S, Lu W and Fu Y 2008 Effects of shape and strain distribution of quantum dots on optical transition in the quantum dot infrared photodetectors *Nanoscale Res. Lett.* **3** 534
[51] Collings P J 1980 Simple measurement of the band gap in silicon and germanium *Am. J. Phys.* **48** 197–9
[52] Kittler M and Reiche M 2011 Structure and properties of dislocations in silicon *Crystalline Silicon- Properties and Uses* ed S Basu (InTech)
[53] Virgilio M and Grosso G 2006 Type-I alignment and direct fundamental gap in SiGe based heterostructures *J. Phys.: Condens. Matter* **18** 1021–31
[54] Conti S, Saberi-Pouya S, Perali A, Virgilio M, Peeters F M, Hamilton A R, Scappucci G and Neilson D 2021 Electron–hole superfluidity in strained Si/Ge type II heterojunctions *npj Quantum Mater.* **6** 41
[55] Dey S, Mukhopadhyay B, Sen G and Basu P K 2018 Type II band alignment in $Ge_{1-x-y}Si_xSn_y/Ge_{1-\alpha-\beta}Si_\alpha Sn_\beta$ heterojunctions *Solid State Commun.* **270** 155–9
[56] Cosentino S, Miritello M, Crupi I, Nicotra G, Simone F, Spinella C, Terrasi A and Mirabella S 2013 Room-temperature efficient light detection by amorphous Ge quantum wells *Nanoscale Res. Lett.* **8** 128
[57] Virgilio M, Schroeder T, Yamamoto Y and Capellini G 2015 Radiative and non-radiative recombinations in tensile strained Ge microstrips: photoluminescence experiments and modeling *J. Appl. Phys.* **118** 233110
[58] Tan T Y and Gösele U 1982 Oxidation-enhanced or retarded diffusion and the growth or shrinkage of oxidation-induced stacking faults in silicon *Appl. Phys. Lett.* **40** 616–9
[59] Niu G *et al* 2016 Dislocation-free Ge nano-crystals via pattern independent selective Ge heteroepitaxy on Si nano-tip wafers *Sci. Rep.* **6** 22709
[60] Kirfel O, Müller E, Grützmacher D, Kern K, Hesse A, Stangl J, Holý V and Bauer G 2004 Shape and composition change of Ge dots due to Si capping *Appl. Surf. Sci.* **224** 139–42
[61] Skoulidis N and Polatoglou H M 2005 Stress distribution, strains and energetics of Si-capped Ge quantum dots: an atomistic simulation study *J. Phys.: Conf. Ser.* **10** 113–6
[62] Hrauda N, Zhang J J, Süess M J, Wintersberger E, Holý V, Stangl J, Deiter C, Seeck O H and Bauer G 2012 Strain distribution in Si capping layers on SiGe islands: influence of cap thickness and footprint in reciprocal space *Nanotechnology* **23** 465705
[63] Wendav T *et al* 2016 Photoluminescence from ultrathin Ge-rich multiple quantum wells observed up to room temperature: experiments and modeling *Phys. Rev.* B **94** 245304
[64] Bogardus E H and Bebb H B 1968 Bound-exciton, free-exciton, band-acceptor, donor-acceptor, and auger recombination in GaAs *Phys. Rev.* **176** 993–1002
[65] Spindler C, Galvani T, Wirtz L, Rey G and Siebentritt S 2019 Excitation-intensity dependence of shallow and deep-level photoluminescence transitions in semiconductors *J. Appl. Phys.* **126** 175703
[66] Kimwing L C 1978 Recombination enhanced defect reactions *Solid-State Electron.* **21** 1391–401
[67] Isometsä J *et al* 2023 Surface passivation of germanium with ALD Al2O3: impact of Composition and crystallinity of GeOx interlayer *Crystals* **13** 667
[68] Cuevas A, Kerr M J and Schmidt J 2003 Passivation of crystalline silicon using silicon nitride *3rd World*

Conference onPhotovoltaic Energy Conversion vol 1 pp 913–8
[69] Dingemans G and Kessels W M M 2012 Status and prospects of Al_2O_3-based surface passivation schemes for silicon solar cells *J. Vac. Sci. Technol. Vac. Surf. Films* **30** 040802
[70] Lieten R R, Bustillo K, Smets T, Simoen E, Ager J W, Haller E E and Locquet J-P 2012 Photoluminescence of bulk germanium *Phys. Rev.* B **86** 035204
[71] Grosse S, Sandmann J H H, Von Plessen G, Feldmann J, Lipsanen H, Sopanen M, Tulkki J and Ahopelto J 1997 Carrier relaxation dynamics in quantum dots: scattering mechanisms and state-filling effects *Phys. Rev.* B **55** 4473–6
[72] Liao Y-A, Hsu W-T, Chiu P-C, Chyi J-I and Chang W-H 2009 Effects of thermal annealing on the emission properties of type-II InAs/GaAsSb quantum dots *Appl. Phys. Lett.* **94** 053101
[73] Dardel B, Grioni M, Malterre D, Weibel P, Baer Y and Lévy F 1992 Temperature-dependent pseudogap and electron localization in 1*T*–TaS_2 *Phys. Rev.* B **45** 1462–5
[74] Liu W, Jiang D, Luo K, Zhang Y and Yang X 1995 Broadening of the excitonic linewidth due to scattering of two-dimensional free carriers *Appl. Phys. Lett.* **67** 679–81
[75] Raymond S, Fafard S, Poole P J, Wojs A, Hawrylak P, Charbonneau S, Leonard D, Leon R, Petroff P M and Merz J L 1996 State filling and time-resolved photoluminescence of excited states in $In_x Ga_{1-x}$ As/GaAs self-assembled quantum dots *Phys. Rev.* B **54** 11548–54
[76] Varshni Y P 1967 Temperature dependence of the energy gap in semiconductors *Physica* **34** 149–54
[77] Manganelli C L, Virgilio M, Montanari M, Zaitsev I, Andriolli N, Faralli S, Tirelli S, Dagnano F, Klesse W M and Spirito D 2021 Tensile strained germanium microstructures: a comprehensive analysis of thermo-opto-mechanical properties *Phys. Status Solidi* a **218** 2100293